CHEMISTRY
A EUROPEAN JOURNAL

DOI: 10.1002/chem.200500542

New Hybrid Bidentate Ligands as Precursors for Smart Catalysts

Frédéric Goettmann,[a, b] Cédric Boissière,[b] David Grosso,[b] François Mercier,[a] Pascal Le Floch,*[a] and Clément Sanchez*[b]

Abstract: 1-Phosphanorbornadiene derivatives were grafted onto various periodically organized mesoporous powders, including a new zirconia/silica mixed oxide synthesized by aerosol techniques. After complexation with the $[Rh(CO)_2]^+$ fragment, these materials were revealed to be more active in olefin hydrogenation than their homogeneous counterparts. The reasons for this higher activity are discussed in the light of theoretical modeling. Various surface treatments, such as esterification, drying, and functionalization with $PhSi(OEt)_3$, provided insights into the nature and mechanism of formation of the active species. Zirconia-based materials were found to be active in internal olefin hydroformylation. Investigation of the mechanism of this reaction shows that the isomerization step is catalyzed by the Lewis acidic support, whereas the hydroformylation step is driven by the rhodium catalyst. Dissociation of these two steps leads to enhancement of activity.

Keywords: hydroformylation · mesoporous materials · P ligands · rhodium · supported catalysts

Introduction

Although homogeneous catalysts are usually more active and selective than heterogeneous ones (apart from metallic nanoparticles), their commercial success lies a long way behind.[1] Indeed, heterogeneous catalysts are easier to handle and can give a more sustainable catalytic process even if they often require more drastic conditions and sophisticated purification techniques. Consequently, much work has been devoted to heterogenization of useful homogeneous catalytic systems, especially organometallic complexes, by using various supports such as clays, polymers, and ceramics.[2] Among these materials, the most widely studied and employed are oxides, particularly silica. Discovery in the early 1990s of periodically organized mesoporous materials[3] opened a new area in the field of supported catalysis: due to their high specific surface and their well-controlled porosity, these materials are suitable for immobilizing catalytic complexes, and have been shown to preserve both the catalytic selectivity and activity, and to allow high reaction rates. Moreover, significant efforts to improve their synthesis by increasing access to the support and presenting more open pore geometries made to fine control of the diffusion of the reactants in the inorganic matrix, and thus accessibility of the catalytic centers, possible.[4]

Two well-known approaches to heterogenization are usually employed[5] (Figure 1): the first, homogeneous supported catalysis, relies on well-defined homogeneous catalysts tethered to a support by an anchoring moiety. To limit interactions between the support and the metal fragment, the anchoring moiety is positioned a long way from the metal center. The second approach, heterogeneous molecular ca-

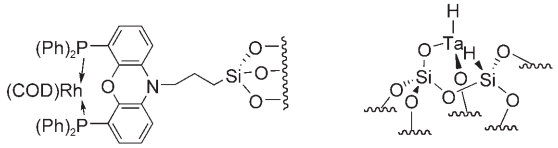

Figure 1. Examples of supported homogeneous catalysts. Left: the anchoring chain consists of a propylsiloxane moiety (ref. [34]). Right: an SOMC catalyst, with the metal directly bonded to the surface (ref. [6]).

[a] F. Goettmann, Dr. F. Mercier, Prof. P. Le Floch
Laboratoire "Hétéroéléments et Coordination"
UMR CNRS 7653 (DCPH), Département de Chimie
Ecole Polytechnique, 91128 Palaiseau Cedex (France)
Fax: (+33) 169-334-570
E-mail: lefloch@poly.polytechnique.fr

[b] F. Goettmann, Dr. C. Boissière, Dr. D. Grosso, Prof. C. Sanchez
Laboratoire de Chimie de la Matière Condensée
Université Pierre et Marie Curie
4 place Jussieu, 75005 Paris (France)
Fax: (+33) 144-274-769
E-mail: clems@ccr.jussieu.fr

Supporting information for this article is available on the WWW under http://www.chemeurj.org/ or from the author.

talysis (or surface organometallic chemistry (SOMC)[6]), exploits the presence of hydroxyl moieties on the surface of the support to bind an isolated metal center to a well-controlled environment.

We recently reported on the synthesis[7] of a new family of mixed P–O grafted ligands that fill the gap between these two approaches, namely hybrid bidentate ligands (HBLs). In this approach, an organic scaffold (the 1-phosphanorbornadiene skeleton) bearing a heteroatom that can coordinate to a transition metal is still present, as in homogeneous supported complexes, but an atom of the anchoring moiety, typically an oxygen atom, also binds the metal center (Figure 2). Since the latter atom is also linked to the surface, these parts of such systems can be regarded as hybrids between classical supported catalysts and SOMC-based catalysts.

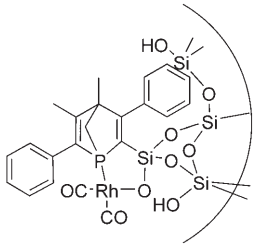

Figure 2. First example of an HBL rhodium complex (ref. [7]) in which the metal center is coordinated by both a purely organic and an inorganic arm.

The proximity of the complex and the pore wall provides a very rigid and well-defined environment for the metal center. Therefore, such bifunctional systems are suitable for studying the influence of pore size and wall effects (curvature, functionalities) on the catalytic activity.[8]

Herein we report on the catalytic behavior of rhodium(I)-based catalysts coordinated by both silica- and zirconia-supported HBLs. For the silica-based materials, both the mechanism of formation and the influence of the functionalization of the wall on the catalytic activity were studied. The synthesis of new zirconia-rich, mesoporous, mixed ZrO_2/SiO_2 powders is described, allowing characterization of a new HBL, namely a grafted phosphanorbornadiene phosphonate derivative. This material was tested in the hydrogenation of alkenes and also found an interesting application in the hydroformylation of 2,3-dimethylbut-2-ene, in which process the Lewis acidity of the wall was exploited to promote alkene isomerization before the rhodium-catalyzed hydroformylation. This new class of hybrid, periodically organized, mesoporous materials built on the surface of binary (or tertiary) mesoporous oxides opens a host of possibilities for the controlled design of smart polyfunctional catalysts.

Abstract in French: *Des dérivés du 1-phosphanorbornadiène ont été greffés sur différents supports mésoorganisés, dont de nouveaux oxydes mixtes silice–zircone produits par aérosol. Ces matériaux, après complexation à des précurseurs de rhodium(I), se sont révélés être des catalyseurs d'hydrogénation des oléfines plus actifs que leurs équivalents homogènes. Les causes possibles de cette augmentation d'activité sont passés à l'aune d'une étude théorique. De plus divers traitements de surface, comme l'estérification des hydroxyls de surface, le séchage, et la fonctionnalisation par $PhSi(OEt)_3$, permettent une meilleure compréhension du mécanisme de formation des espèces actives. Les matériaux à base de zircone se sont avérés être actifs en hydroformylation des oléfines internes. L'étude du mécanisme de cette catalyse montre que l'étape d'isomérisation de l'oléfine est catalysée par la zircone alors que l'hydroformylation l'est par le complexe de rhodium. Le fait que ces deux étapes soient réalisées par des catalyseurs différents explique la bonne activité observée.*

Results

Synthesis of the anchorable phosphanorbornadiene species

*1-Phospha-2-triethoxysilyl-4,5-dimethyl-3,6-diphenylnorbornadiene (**2**)*: Synthesis of **2** was achieved by a well-known procedure that relies on the reactivity of 2*H*-phospholes toward functional alkynes (e.g., **1**) (Scheme 1).[9] Importantly, the [4+2] cycloaddition process was very regioselective, due to the electronic properties of the alkoxysilyl moieties. As explained previously,[7] **2** behaved as a bidentate ligand toward rhodium(I) precursors and variable-temperature ^{1}H NMR experiments on the complex $[Rh(cod)_2][PF_6]$ (cod = cyclooctadiene) showed that the three ethoxy moieties exchange rapidly in solution with a coalescence temperature of −20 °C.

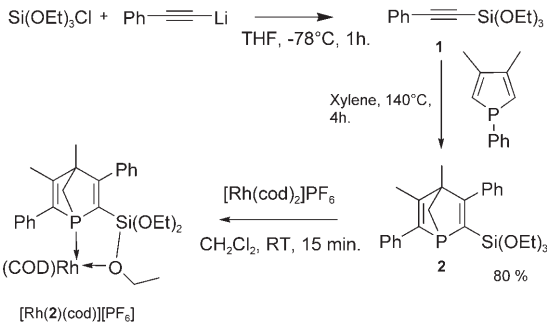

Scheme 1. Synthesis of anchorable phosphine **2**.

*1-Phospha-2-triethoxysilyl-4,5-dimethyl-3,6-diphenylnorbornene (**2′**)*: In ligand **2**, the protons around the siloxane moiety are not numerous enough to provide efficient CP-MAS ^{29}Si NMR measurements once grafted. Therefore the 1-phosphanorbornene **2′** was synthesized (see Scheme 2), assuming that it would display the same grafting ability as **2**. (The liquid ^{29}Si NMR signal had quite a low chemical shift (−49.6) for an alkyltriethoxysilane.

*1-Phospha-2-ethoxydimethylsilyl-4,5-dimethyl-3,6-diphenylnorbornadiene (**4**)*: Compound **4** was synthesized by the same procedure as for **2** (Scheme 3), by using ethoxydime-

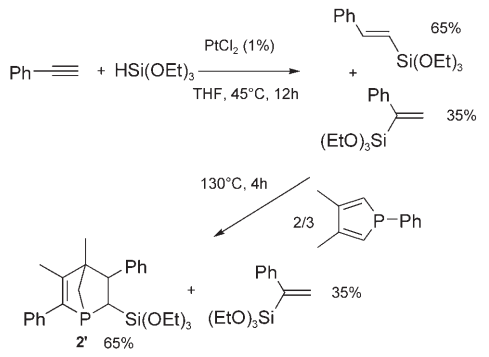

Scheme 2. Synthesis of model phosphine **2′**.

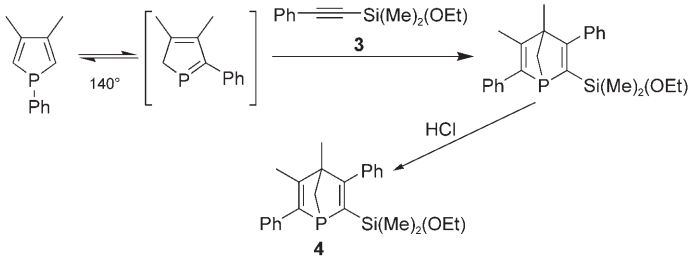

Scheme 3. Synthesis of a methylated derivative (**4**) of **2**.

thyl(phenylethynyl)silane (**3**), which was readily prepared by reaction of one equivalent of chlorodimethyl(phenylethynyl)silane[10] with one equivalent of ethanol in THF. Compound **4** was fully characterized by NMR techniques.

*1-Phospha-4,5-dimethyl-3,6-diphenylnorbornadienylphosphonic acid (**5**)*: The synthesis of phosphanorbornadiene **5** has already been reported.[11] It was also shown that it behaves as a bidentate ligand toward rhodium(I) precursors. These complexes were used as water-soluble hydroformylation catalysts but exhibited a low activity.

*1-Oxo-1-phospha-4,5-dimethyl-3,6-diphenylnorbornadienylphosphonic acid (**5′**)*: This was synthesized by HNO_3 oxidation of **5** in methanol (Scheme 4). It was characterized by NMR and IR techniques.

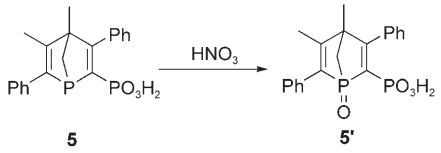

Scheme 4. Synthesis of the oxide of **5**.

Synthesis of the supporting material

Silica materials: The silica materials used have all been described previously. The first, of the **SBA-1** type,[12] was synthesized under acidic conditions in the presence of cetyltriethylammonium bromide (CTEAB) as surfactant. It had a specific surface area of 750 $m^2 g^{-1}$, an average pore diameter of 23 Å, and a cubic (**SBA-1**) pore structure organization. The second was a standard **SBA-15** type support[13] with surface area 630 $m^2 g^{-1}$, pore diameter 60 Å; the pore structure had a hexagonal (p6m) arrangement. The last one was an **MSU** type of support, specific surface area 310 $m^2 g^{-1}$, average pore diameter 110 Å.[14]

Mixed zirconia/silica materials: Mesoporous ZrO_2/SiO_2 mixed oxides are of growing importance as they provide enhanced mechanical and chemical stability compared with their pure zirconia counterparts.[15] This is the first reported synthesis of such materials using standard aerosol techniques. In this work, we focused on obtaining final material with high zirconia loadings. Preparation of the sol has been reported previously for synthesis of thin films.[16] The atomization sol was prepared by mixing a Zr-containing sol (Sol A), molar ratio $ZrCl_4$/EtOH/surfactant = 1:40:*c*, and a given volume of a Si-containing sol (Sol B), molar ratio $SiCl_4$/EtOH/surfactant = 1:40:*c*, fixing the Zr/Si ratio. The surfactant loading depended on the nature of the surfactant. Water was added just before atomization in a ratio H_2O/(Zr+Si) = 10:1. The aerosol was then generated using a commercial atomizer with dry air as atomization gas. The resulting powders were labeled $\mathbf{ZS}x_{\mathbf{(S)}}$ (in which x = Si loading [mol%], ranging from 0 to 30; (S) = surfactant; (S) = F for F127 or (S) = C for cetyltrimethylamonium bromide (CTAB)).

When using a Pluronic surfactant (F127), as for the synthesis of thin layers, the transmission electronic micrographs (TEMs) and the XRD pattern showed a monodisperse porosity ($2\theta = 0.94$ for $\mathbf{ZS20_F}$). However, upon calcination at 300 °C the powders became dark brown and FT-IR spectra revealed the formation of carbonates, resulting from incomplete oxidation of organics. At higher temperature (450 °C), the specific surface dropped dramatically (from 110 $m^2 g^{-1}$ to <5 for $\mathbf{ZS20_F}$, for example). The porosity of $\mathbf{ZS10_F}$ and $\mathbf{ZS20_F}$ before calcination is shown in Figure 3.

This calcination step was avoided by using CTAB as a surfactant, which can be removed by ethanol washing after 24 h of consolidation at 130 °C. Using CTAB, we were able to synthesize mixed oxide aerosols with x ranging from 0 to 30%. Specific surface areas of the powders obtained were fairly high (230–470 $m^2 g^{-1}$; see Table 1) for zirconium-rich metal oxide porous powders. Average pore sizes were rather small, even with $\mathbf{ZS20_C}$, but this is in good agreement with the well-established sintering of zirconia-rich materials during consolidation.[16] Structural characteristics of the zirconia/silica mixed powders are presented in Table 1 and TEMs of a pure zirconia powder, $\mathbf{ZS10_C}$, $\mathbf{ZS20_C}$, and $\mathbf{ZS30_C}$ are shown in Figure 4.

Synthesis of the grafted materials

Grafting on the silica supports: The same procedure was used for the three supports. Ligand **2** (**2′**) was added to a

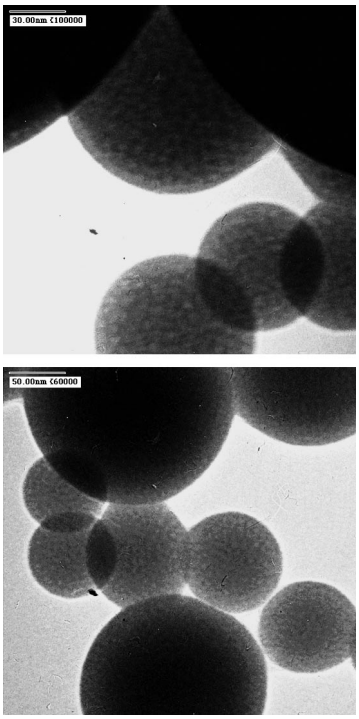

Figure 3. TEMs of $\mathbf{ZS10}_{\mathbf{F127}}$ (top) and $\mathbf{ZS20}_{\mathbf{F127}}$ (bottom), showing the porosity before calcination.

Table 1. Characteristics of the zirconia/silica mixed powders.

	Silica content [%]	Specific surface area [$m^2 g^{-1}$]	BJH average pore diameter [Å]	XRD[a] *d* spacing [nm]
$\mathbf{ZS0}_{\mathbf{C}}$	0	470	<10	–
$\mathbf{ZS10}_{\mathbf{C}}$	10	320	<20	4.2
$\mathbf{ZS20}_{\mathbf{C}}$	20	230	20	5.5
$\mathbf{ZS30}_{\mathbf{C}}$	30	230	<10	–

[a] X-ray diffraction.

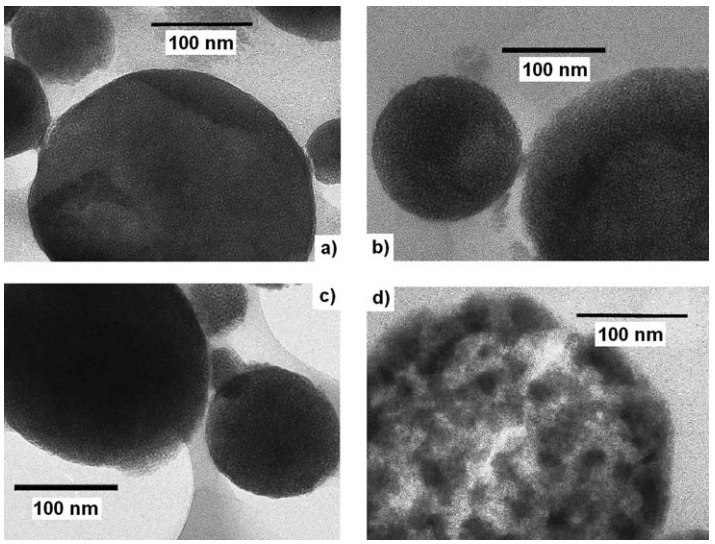

Figure 4. TEMs of a) pure zirconia powder; b)$\mathbf{ZS10}_{\mathbf{C}}$; c) $\mathbf{ZS20}_{\mathbf{C}}$; d)$\mathbf{ZS30}_{\mathbf{C}}$.

suspension of the corresponding support in toluene at room temperature and then stirred at 90 °C for 12 h. The resulting materials are labeled **2@SBA-1**, **2′@SBA-1**, **2@SBA-15**, and **2@MSU**. The ligand loading was checked by thermogravimetric analysis (TGA) and 14, 12, 6, and 8 wt %, respectively, of the organic compound was grafted. The CP-MAS ^{1}H NMR characterizations of **2@SBA-1** showed that there were few ethoxy groups left on the surface, indicating that the grafting was almost complete. This was confirmed by CP-MAS ^{29}Si NMR experiments on **2′@SBA-1**, in order to obtain good cross-polarization yields. The chemical shift ($\delta = -75$ ppm) was consistent with a species which is triply bonded (T3) to the surface, relative to its $\delta = -49.61$ ppm shift before grafting. Though the CP experiments are not quantitative, the CP-MAS ^{31}P NMR spectrum indicated that a large part of the phosphine remained unoxidized ($\delta = -8$ ppm).

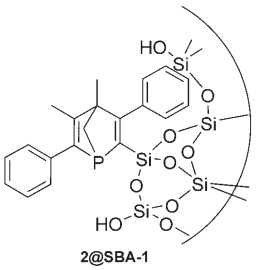

2@SBA-1

Grafting on the zirconia-rich supports: Although grafting of phosphonic-based species on zirconia-rich materials should be easier than for the silica equivalents, because of the small pore size of $\mathbf{ZS20}_{\mathbf{C}}$, we applied the same grafting procedure as for **2@SBA-1**. The grafting was followed by ^{31}P NMR spectroscopy of the solution, with Ph_3P as internal standard. After 12 h of heating detectable traces neither of **5** nor of **5′** were found in solutions corresponding to a 20 wt % loading. The CP-MAS ^{31}P NMR spectrum of $\mathbf{5@ZS20}_{\mathbf{C}}$ showed two large main peaks at $\delta = 3.5$ and 54 ppm, which were ascribed to the phosphonate moiety[17] and to the phosphine, respectively. Interestingly, the second chemical shift ($\delta = 54$ ppm) is shifted significantly downfield relative to that recorded for the free ligand ($\delta = -9$ ppm). Usually, such a downfield shift indicates that the phosphorus atom has been oxidized. However, the FT-IR spectra of $\mathbf{5@ZS20}_{\mathbf{C}}$ and $\mathbf{5'@ZS20}_{\mathbf{C}}$ are distinct, providing clear evidence that $\mathbf{5@ZS20}_{\mathbf{C}}$ is not in an oxidized state. In particular the characteristic absorption band of the P=O bond (at 1380 cm^{-1}) is missing in the spectrum of $\mathbf{5@ZS20}_{\mathbf{C}}$. (As described previously for phosphonates grafted on titania,[18] no phosphonate P=O bands are visible around 1200 cm^{-1}, whereas the P–O–Zr bands are visible around 1100 cm^{-1} together with the signal of the support; Figure 5).

Another possible explanation for this downfield shift is that the phosphine was protonated by the acidic zirconia surface. However, parallel experiments led us definitely to rule out this hypothesis. Indeed, even when it was dissolved in aqueous 12 M HCl, ligand **5** proved to be very difficult to protonate and only a very weak signal (compared with that of nonprotonated **5**) was detected at $\delta = 8$ ppm in the ^{31}P NMR spectrum. This chemical shift is consistent with the tabulated value. For example, in $ClPH(Ph)_3$ the phosphorus

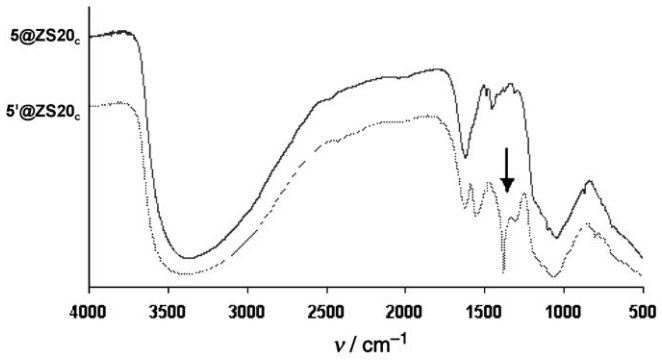

Figure 5. FT-IR spectra of **5@ZS20$_C$** and **5′@ZS20$_C$**. Note the strong peak at 1380 cm^{-1} (arrow) characteristic of $R_3P{=}O$ vibrations.

atom resonates at $\delta = 0$ ppm.[19] The third hypothesis is that the phosphorus atom of the grafted ligand **5** can coordinate with the zirconia surface. Interestingly, ^{31}P NMR experiments indicated that reaction of two equivalents of **5** with $ZrCl_4$ in EtOH led to the formation of a new peak at $\delta =$ 61 ppm (−5 ppm for the phosphonate moiety). This downfield chemical shift is consistent with that recorded for **5@ZS20$_C$**. Therefore, it seemed reasonable to assume that **5@ZS20$_C$** adopts the structure shown here (the locations of the phosphonate oxygen atoms are not exact). The coordination of the phosphorus atom with the surface probably explains why no oxidation takes place.

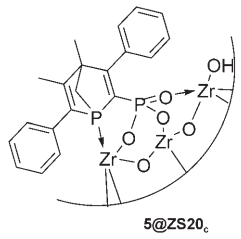

5@ZS20$_c$

This assumption was reinforced by additional solid-state NMR experiments. We supposed that if a coordination of the phosphorus atom with the zirconia surface occurred, the resulting bond would probably be weak because of the poor affinity of tertiary phosphines for Zr^{IV} centers. Thus displacement reactions were attempted using alkynes which can act as ligands to Zr^{IV} centers through their π system.[20] As expected, reaction of **5@ZS20$_C$** with an excess of phenylacetylene for 12 h resulted in the appearance in solid-state ^{31}P NMR spectrum of a new signal at $\delta = -8$ ppm, which corresponds to the free phosphine moiety of **5**.

Synthesis of surface-modified grafted material

(2+OMe)@SBA-1: In order to check the influence of the functionalization of the surface on the catalytic activity, **2@SBA-1** was esterified by suspending the material for 1 h at 45 °C in methanol. Modification of the surface was confirmed by a 1.5 wt % uptake in TGA.

(2+Ph)@SBA-1, ***(2+Ph)@MSU***: Similarly, **2@SBA-1** and **2@MSU** were treated with $PhSi(OEt)_3$ at 90 °C in toluene for 12 h. This resulted in an uptake of 6 wt % for both supports. **(2+Ph)@MSU** was dried for 24 h in vacuo at 60 °C to yield **(2+Ph)@MSU$_d$**. However, such a surface treatment does not usually result in complete drying or in isolated OH groups, as this requires more drastic conditions.[21] Heating at higher temperature (120 °C), however, led to total passivation of the catalytic material.

Complexation of the solids: The grafted materials were suspended in CH_2Cl_2 with a given amount of rhodium(I) precursor, $[Rh(cod)_2][PF_6]$ or $[Rh(acac)(CO)_2]$, and then washed three times with MeOH, yielding the corresponding [Rh(ligand)]@solid compounds.

[Rh(2)(cod)]@SBA-1: The CP-MAS ^{31}P NMR spectrum exhibited a single peak at $\delta = 58$, consistent with the spectrum of **6** (the structure of which is illustrated here; the other ligands on the rhodium center are omitted). No signal corresponding to the $[PF_6^-]$ counter anion could be detected.

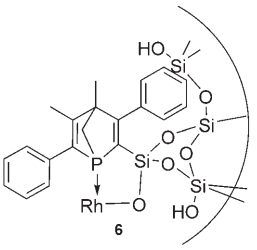

6

[Rh(2)(CO)$_2$]@SBA-1: The FT-IR spectrum of the material obtained with **2@SBA-1** when using $[Rh(acac)(CO)_2]$ as a precursor clearly indicated that a displacement of the acac ligand occurred (the two CO ligands featuring two characteristic bands at 2002 and 2074 cm^{-1}). These data corroborate the assumption that the ligand also behaves as a bidentate P^O$^-$ chelate.

[Rh(5)(CO)$_2$]@ZS20$_C$: For this support, only $[Rh(acac)(CO)_2]$ was used as a precursor. CP-MAS ^{31}P NMR spectroscopy showed that the peak at $\delta = 54$ ppm in **5@ZS20$_C$** shifted to $\delta = 58$ ppm (the same chemical shift as for [Rh(**2**)(cod)]@**SBA-1**). FT-IR spectroscopy showed that the acac ligand was not eliminated, since it can also act as a ligand for the zirconia surface.[22] However, the shift of the two C=O stretching bands (1590 and 1538 cm^{-1} on the solid instead of 1564 cm^{-1} and 1527 cm^{-1} in $[Rh(acac)(CO)_2]$) clearly indicates that it has been displaced by the grafted ligand **5** (**5@ZS20$_C$**), which thus acts as a bidentate P^O$^-$ chelate.

Catalytic tests: The catalytic activity of the supported catalysts that had been prepared was evaluated in two processes: the hydrogenation of 1-hexene and the hydroformylation of 2,3-dimethylbut-2-ene. All the homogeneous complexes were formed in situ whereas all the supported complexes were synthesized before being used as catalysts.

Hydrogenation of 1-hexene: All these tests were at room temperature under H_2 (7 bar). The metal/substrate ratio was set at 1:1000.

Homogeneous catalysis: All the experiments were performed using MeOH as solvent. As complex [Rh(**2**)(cod)]-

$[PF_6]$ proved to be inactive in the hydrogenation of hexene, complex $[Rh(\mathbf{4})(cod)][PF_6]$ was tested in order to avoid the exchange of the ethoxy moieties. A very low activity was observed, combined with a long activation period (around 40 min). The addition of 1 equiv of water to $[Rh(\mathbf{4})(cod)][PF_6]$ resulted in the breaking of the Si–O bond, yielding a P^O$^-$ chelate (Scheme 5). Indeed, the ^{31}P signal of the complex shifts from $\delta = 52.8$ to 52.4 ppm, whereas the release of ethanol is clearly visible in the ^1H spectrum (complexed Si–OEt moieties feature a quadruplet of doublets at $\delta =$ 3.5 ppm with $^3J(H,H) = 5$ Hz and $^3J(H,Rh) = 1$ Hz, whereas after hydrolysis a quadruplet appears at $\delta = 3.7$ ppm with $^3J(H,H) = 7$ Hz) The neutral complex had the same activity as the cationic one but no activation period was needed. The hydrogen consumption in the two experiments is presented in Figure 6.

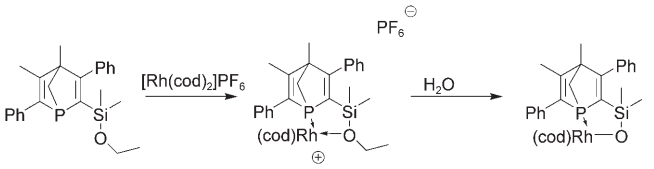

Scheme 5. Formation of the active species in the hydrogenation of 1-hexene with $[Rh(\mathbf{4})(cod)]PF_6$.

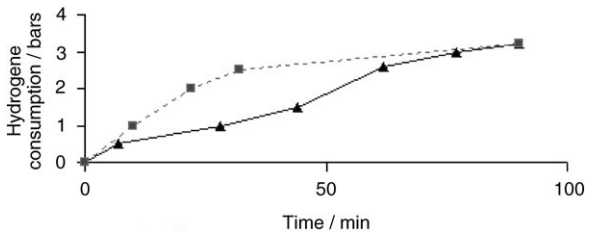

Figure 6. Hydrogen consumption during the hydrogenation of 1-hexene with $[Rh(\mathbf{2}')(cod)][PF_6]$: ▲ without addition of water; ■ with pre-hydrolysis.

Heterogeneous catalysis: The substrate/catalyst ratio (calculated on the basis of the theoretical rhodium loading) was set at 1000:1. The dry catalytic powders were suspended in the solution containing the substrate before pressurization. The most interesting catalytic activities are summarized in Table 2.

The solids behaved well during recycling, as previously mentioned.[7] The powders only had to be filtered off and could be re-used directly in a new catalytic batch. By this procedure a maximum TON of more than 100000 catalytic cycles for $[Rh(\mathbf{2})(cod)]$@**SBA-1** was reached (without any notable activity loss after 20 recycles).

Table 2. Turnover frequencies [cycles min^{-1}] for the catalytic hydrogenation of 1-hexene.

Entry	Catalyst	MeOH	Toluene
1	$[Rh(\mathbf{2})(cod)]$@**SBA-1**	48	4
2	$([Rh(\mathbf{2})(cod)] + OMe)$@**SBA-1**	–[a]	10
3	$[Rh(\mathbf{2})(cod)]$@**SBA-15**	72	–
4	$[Rh(\mathbf{2})(cod)]$@**MSU**	10	–
5	$[Rh(\mathbf{5})(CO)_2]$@**ZS 20$_C$**	30	–
6	$([Rh(\mathbf{2})(cod)] + Ph)$@**SBA-1**	15	30
7	$([Rh(\mathbf{2})(cod)] + Ph)$@**MSU**	12	12
8	$([Rh(\mathbf{2})(cod)] + Ph)$@**MSU$_d$**	15	4.6
9	$([Rh(\mathbf{2})(cod)] + Ph)$@**MSU$_d$**[b]	–	10.3

[a] Empty entries (–) correspond to conditions that were not tested. [b] Catalytic activity after addition of water ($Rh/H_2O = 1:1$).

Hydroformylation of 2,3-dimethylbut-2-ene

Hydroformylation catalysis: To check whether the Lewis acidic properties of the zirconia-rich wall of **ZS 20$_C$** could be advantageous for difficult reactions, $[Rh(\mathbf{5})(CO)_2]$@**ZS 20$_C$** was tested in the hydroformylation of 2,3-dimethylbut-2-ene, a substrate known to be rather reluctant to undergo hydroformylation. In this reaction, isomerization into 2-methyl-3,3′-dimethylprop-1-ene takes place before the hydroformylation, which yields 3,4-dimethylpentanal (Scheme 6).[23]

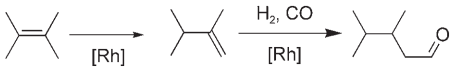

Scheme 6. Principle of the 2,3-dimethylbut-2-ene hydroformylation.

The results obtained after 48 h in experiments with 0.1 mol% of catalyst at 110°C under H_2/CO (1:1, 30 bar), summarized in Table 3, demonstrate that the supporting material itself is active in isomerization of the internal olefin (entry 1). The homogeneous catalyst is about four times less active than the supported one (entries 2 and 3).

Table 3. Hydroformylation of 2,3-dimethylbut-2-ene.

	Catalyst	Isomerization rate[a] [%]	Aldehyde selectivity[b] [%]	Linearity[c] [%]
1	**ZS 20$_C$**	30	3	100
2	$[Rh(\mathbf{5})(CO)_2]$	0	10	100
3	$[Rh(\mathbf{5})(CO)_2]$@**ZS 20$_C$**	0	40	100

[a] Total percentage of 2,3-dimethylbut-1-ene formed. [b] Total percentage of aldehyde formed. [c] 3,4-Dimethylpentanal formed as a percentage of the total aldehydes formed.

Discussion

Nature of the active species: The activation period (40 min) observed when the $[Rh(\mathbf{2}')(cod)][PF_6]$ complex was used as the catalyst strongly suggests that the active species is probably not the cationic species. Indeed, as previously explained, hydrolysis of this complex clearly promoted the hydrogenation process. Though CP-MAS Si^{29} NMR experimental data showed that **2@SBA-1** was triply bonded through to oxygen atoms on the surface, NMR and IR re-

sults clearly suggest that **2@SBA-1** behaves as an LX-type ligand. Therefore, a Si–O bond must open during or just after the complex formation, giving rise to the active species. This assumption is supported by the catalytic tests on ([Rh(**2**)(cod)]+Ph)@**MSU$_d$**. Indeed, when a dried catalyst was used in toluene as solvent, the activity was found to be much lower (4.6 catalytic cycles per minute) than when methanol was used as solvent (15 catalytic cycles per minute). Interestingly, when a wet catalyst was used the activity was found to be comparable whatever the solvent used (see Table 2, entry 7). This observation can be rationalized by considering that methanol is able to break Si–O–Si bonds (esterification of the surface).[24] This Si–O bond breaking may be facilitated by coordination of one oxygen lone pair to the rhodium center (Scheme 7). Furthermore, the catalytic activity was observed to increase (10.3 cycles per minute, comparable with the wet catalyst) when water was added to the batch containing the dried catalyst in toluene and the batch was reloaded (Table 2, entry 9).

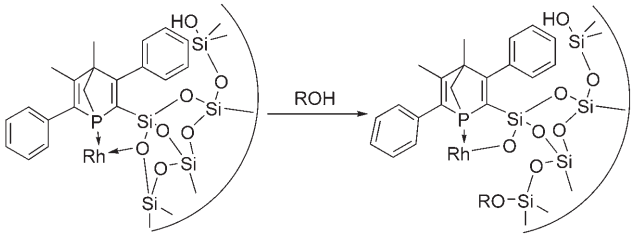

Scheme 7. Formation of the active species through breaking of an Si–O bond by H_2O or an alcohol. The other ligands on rhodium have been omitted.

To gain insight into the influence of the bonding in the active species, DFT calculations were performed using the Gaussian O3 package with the B3PW91 functional. For details of the combination of basis sets used, see the Experimental Section. The model complexes **I** and **II** were optimized. For simplification the phenyl moieties of the corresponding complexes were replaced by hydrogen atoms and the ethoxy moieties by methoxy fragments, and neither the counter ion nor other ligands were considered in these calculations. Complex **I** is a cationic 14 VE (valence electron) complex in which coordination of the rhodium center occurs through the lone pair at phosphorus and one lone pair of one oxygen atom of the Si(OMe)$_3$ group. In the neutral 14 VE complex **II**, which models the proposed active species, the ligand behaves as an LX ligand. The two optimized structures are presented in Figure 7 and the most significant bond lengths and bond angles are listed in Table 4.

Interestingly, a natural bond analysis of the optimized structures revealed that, in complex **I**, coordination of one lone pair on the Rh center only slightly reduces the negative charge at the coordinated oxygen atom (−0.86 in **I**; −0.90 for an uncoordinated oxygen atom). A lengthening of the

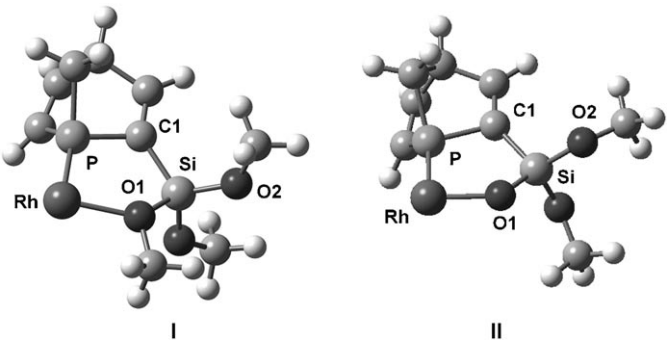

Figure 7. Optimized structures of models of complexes **I** and **II**.

Table 4. Comparison of the most interesting bond lengths [Å] and angles [°] in the model complexes **I** and **II**.

	I	**II**
P–Rh	2.196	2.189
O1–Rh	2.111	1.947
Si–O1	1.725	1.662
Si–O2	1.638	1.830
P-Rh-O1	47.5	91.5
C1-P-Rh-O1	−1.6	1.6

Si–O bond is also noted (1.726 Å in **I**; 1.621 Å for an uncoordinated oxygen atom). Though these variations are relatively small, they reinforce the hypothesis that upon coordination to Rh the Si–O bonds are weakened. The natural charge at rhodium in both model complexes **I** and **II** is also important. Coordination of the oxygen atom in a covalent manner results in a small decrease in the positive charge at rhodium (+0.23 in **II**; +0.28 in **I**) (see Figure 8). However, this increase in the electron density on the Rh center is too modest to explain the enhancement of the catalytic activity on going from the cationic to the neutral complex.

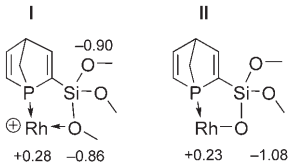

Figure 8. NBO charge distribution in complexes **I** and **II**.

Thus the effects of the oxygen and the phosphorus atom of the phosphanorbornadiene on possible ligands in *trans* positions were also investigated. For this purpose, structures **III** and **IV**, both featuring two coordinated ethylene ligands at rhodium, were optimized at the same level of theory. The C3–C4 ligand is *trans* to the oxygen ligand and the C4–C5 one *trans* to the phosphorus atom of the phosphanorbornadiene. For a view of the optimized structures see Figure 9; the most significant bond distances and angles are listed in Table 5.

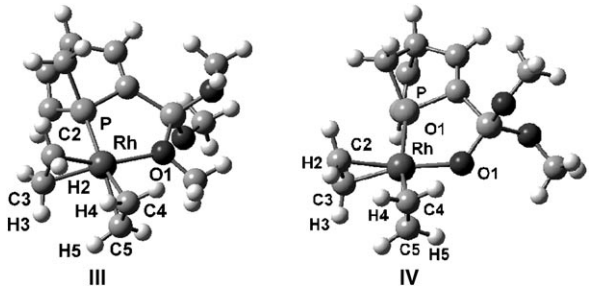

Figure 9. Optimized structures of models of complexes **III** and **IV**.

Table 5. Comparison of the most interesting bond lengths [Å] and angles [°] in the model complexes **III** and **IV**.

	III	IV
P–Rh	2.312	2.319
O1–Rh	2.290	2.045
Rh–C2	2.122	2.126
Rh–C3	2.121	2.127
C2–C3	1.399	1.399
H2-C2-C3-H3	153.32	153.05
Rh–C4	2.247	2.224
Rh–C5	2.241	2.221
C4–C5	1.367	1.371
H4-C4-C5-H5	162.948	164.59

Interestingly, it appears that the effect of the oxygen ligands, whatever the charge at the rhodium center, is similar. The olefin that is *trans* to the oxygen is more strongly bonded to the rhodium center, whereas the olefin *trans* to the P atom is more weakly bonded. This is clearly apparent from the Rh–C bond lengths which are always shorter for the C2–C3 coordinated olefin, reflecting a stronger π back-bonding. Concomitantly, this shortening is accompanied by a lengthening of the C–C bond (for example, in **III**: from 1.399 Å for C2–C3 to 1.367 Å for C4–C5). Evidence for the stronger π back-donation in the C2–C3 olefin is also provided by a decrease in the dihedral angle H2-C2-C3-H3 compared with H4-C4-C5-H5. However, a conclusion about the respective effect of oxygen ligands in the two structures is much more difficult to reach. The results of an NBO (natural bond orbital) analysis are presented in Figure 10. In contrast to compound **II**, covalent coordination of the oxygen ligand increases the positive charge at rhodium. This indicates a better electronic transfer to the C2–C3 olefinic ligand, which is more negatively charged in **IV** than in **III**.

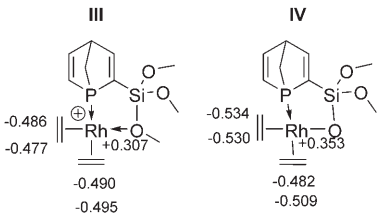

Figure 10. NBO charge distribution in complexes **III** and **IV**.

Though some electronic differences exist between **I** and **II** and between **III** and **IV**, it is clear that all these data cannot account definitely for the higher catalytic activity of complex **II** since the differences are so subtle. A possible explanation may reside in the strain provided by the metallacycle Rh-P-Si-O in **II** and **IV**. Indeed, whereas the oxygen ligand is covalently bonded in **II**, the Si-O-Me group in **I** probably acts as a hemilabile ligand, thus transiently leaving a poorly coordinated and probably highly reactive rhodium center. Further calculations are currently in progress to confirm this hypothesis.

Influence of the surface functionalization: One important factor controlling the activity of a heterogeneous catalyst is the accessibility of the catalytic sites. The turnover frequency of a support with small pores and high tortuosity such as **SBA-1**, with a cubic *Pm3n* structure, is lower (48 cycles per minute) than that of a more open one like **SBA-15**, of 2D hexagonal structure (72 cycles per minute). However, accessibility is directed not only by the pore geometry, but also by the interaction between the reactants and the surface of the support. The high hydrophilicity of mesoporous silica gels synthesized under acidic conditions[25] accounts for the rather low activity observed with [Rh(**2**)(cod)$_2$]@**SBA-1** in toluene, which is quite a classic solvent for homogenous hydrogenation (Table 2, entry 1). When methanol is used as solvent, esterification of the silica surface takes place, making it more hydrophobic and thus increasing the activity. This is emphasized by the fact that with a material pretreated with methanol, the catalysis conducted in toluene (entry 2 in Table 2) is about two times faster. When a mesoporous silica-based material treated with PhSi(OEt) is used (entry 6 in Table 2), the influence of the affinity between the surface and the solvent becomes even more pronounced as the activity in toluene is two times greater than in methanol.

Influence of the chemical nature of the wall: A zirconia-rich material does not seem to alter the catalyst behavior for hydrogenation notably. As shown by DFT calculations, the charge on the rhodium center is slightly higher with ligand **5** than with the hydrolyzed ligand **2**. The mean pore diameter is also slightly smaller in **ZS20$_C$** than in **SBA-1**. Both factors tend to make [Rh(**2**)(CO)$_2$]@**SBA-1** a much more active catalyst. Surprisingly the difference between the latter catalyst and [Rh(**5**)(CO)$_2$]@**ZS20$_C$** is quite small (48 min^{-1} versus 30 min^{-1}). This could be explained by the good affinity of carbon–carbon double bonds for Lewis acids. If the association constant between the hexene molecules and the acidic sites of the zirconia surface is high enough, the diffusion mechanism can be seen as a two-dimensional rather than a standard three-dimensional one. According to this model, the substrate moves onto the surface rather than being in the solution, and thus the probability of meeting the active center is enhanced.

Homogeneous tandem catalysts have attracted great interest in recent years, in particular for industrial applications:[26] indeed, they allow one-pot multistep reactions with-

out the expensive and fastidious product separation steps. The main drawback of a homogeneous approach is that incompatible catalysts, such as bases and acids, cannot be used. Anchoring of such catalysts on a solid support circumvents these problems. The most important papers in this field report the anchoring of two catalytic entities on the same support[27] or the use of an inorganic solid which itself has two different catalytic properties.[28] Bifunctionality in the case of [Rh(**5**)$(CO)_2$]@**ZS20$_C$** relies both on the presence of a rhodium center acting as an hydroformylation catalyst and on the Lewis acidic properties of the wall. The latter property can be exploited in the isomerization of internal olefins to yield linear aldehydes. As is evident in the hydroformylation of 2,3-dimethylbut-2-ene, zirconia alone is able to isomerize alkenes whereas the nongrafted rhodium complex does not yield any isomerization product and is inefficient as a catalyst. This comparison confirms that the isomerization process is the slow step of the catalytic cycle. In contrast, [Rh(**5**)]@**ZS20$_C$** is able to perform both transformations simultaneously. Though the resulting bifunctional catalyst compares with other reported homogeneous systems,[23] the concept in itself is new.

Conclusion

We have shown here that hydride bidentate ligands (HBLs) are new materials that are able to bond to transition metals and to act as very efficient catalysts. The range of characterization techniques that can be used, including kinetic studies, allows good identification both of the complexes formed and of the active species. The synthesis of mixed zirconia/silica powders with a periodically organized mesoporosity by an aerosol technique provides a convenient method for the elaboration of supports that present additional Lewis acidic properties (compared with standard silica). Moreover, the use of ligands such as phosphines or amines bearing phosphonate or carboxylate moieties opens up a new branch of HBLs with promising catalytic properties, as confirmed by the behavior of [Rh(**5**)]@**ZS20$_C$**. Indeed, multifunctional catalysis can be driven very easily by a suitable combination of the catalytic properties of both the grafted complex and the wall.

Experimental Section

All reactions were performed routinely under an inert atmosphere of argon or nitrogen by Schlenk techniques and using dry deoxygenated solvents. Dry THF and hexanes were obtained by distillation from Na/benzophenone. Dry dichloromethane was distilled on P_2O_5 and dry toluene on metallic Na. NMR spectra were recorded on a Bruker AC-200 SY spectrometer operating at 300.0 MHz for ^{1}H, 75.5 MHz for ^{13}C, and 121.5 MHz for ^{31}P. Solvent peaks have been used as internal references relative to Me_4Si for ^{1}H and ^{13}C chemical shifts; ^{31}P chemical shifts are relative to an 85% H_3PO_4 external reference. Powder XRD spectra were recorded on a Philipps PW 1830. BET analyses were recorded on a Micromeritics ASAP 2000. IR spectra in KBr were recorded on a Nicolet Magna 550. Thermogravimetric analyses were carried out on a TA SDT6960 instrument, from RT to 1000 °C at 5 °C min^{-1}. Solid-state ^{31}P NMR spectra were recorded on a Brucker Avance 300 (7.6 T, 300 MHz for ^{1}H, 121 MHz for ^{31}P) at a spinning rate of 14 kHz. Butyllithium in ether solution was purchased from Aldrich.

Triethoxy(phenylethynyl)silane (1): BuLi (6.25 mL, 1.6 M solution in hexanes, 10 mmol) was added carefully to a solution of phenylacetylene (1.02 g, 10 mmol) in THF (15 mL) at −70 °C with vigorous stirring. The solution was allowed to warm slowly to room temperature. After 2 h the dark brown reaction mixture was added slowly to a solution of chlorotriethoxysilane (1.98 g, 10 mmol) in THF (15 mL) at 0 °C. After being allowed to warm again to RT, the solvents were removed in vacuo. The LiCl salts were precipitated with hexanes and filtered off. The hexanes were removed in vacuo, then the product was purified by Kugelrohr distillation (160 °C at 10 mm) yielding a colorless oil. Yield: 2.5 g (95%); ^{1}H NMR ($CDCl_3$, 300 MHz): $\delta = 1.3$ (t, ^3J(H,H) = 7 Hz, 9H; CH_3), 3.9 (q, ^3J(H,H) = 7 Hz, 6H; OCH_2), 7.3 (m, 3H; CH of phenyl), 7.5 ppm (m, 2H; C_{para}H of phenyl); ^{13}C NMR ($CDCl_3$, 75.5 MHz): $\delta = 18.4$ (s, CH_3), 59.5 (s, OCH_2), 85.4, 104.5 (2 s, C of the alkyne), 122.3 (s, C_{ipso} of the phenyl), 128.7–132.8 ppm (3s, C of the phenyl); MS (IE): m/z: 263 [M^+].

1-Phospha-2-triethoxysilyl-4,5-dimethyl-3,6-diphenylnorbornadiene (2): A solution of **1** (1.32 g, 5 mmol) and 1-phenyl-3,4-dimethylphosphol (0.96 g, 5 mmol) in xylene (5 mL) were heated together in a sealed tube at 140 °C for 4 h. The reaction mixture was filtered over celite and xylene was removed in vacuo. The product was isolated as a colorless oil. Yield: 2 g (90%); ^{1}H NMR ($CDCl_3$, 300 MHz): $\delta = 0.9$ (t, ^3J(H,H) = 7 Hz, 9H; CH_3), 1.3 (s, 3H; CH_3), 1.9 (m, 2H; CH_2), 2.0 (s, 3H; vinylic CH_3), 3.5 (q, ^3J(H,H) = 7 Hz, 6H; OCH_2), 7.0, 7.2–7.5 ppm (d, J(H,H) = 7 Hz, 2H; m, 8H; phenyls); ^{13}C NMR ($CDCl_3$, 75.5 MHz): $\delta = 16.3$ (s, vinylic CH_3), 18.5 (s, CH_3 of the ethoxy moieties), 20.9 (s, CH_3), 59.5 (s, OCH_2), 67.3 (s, CH_2), 73.9 (s, C3), 125.5–128.7 (4s, aromatic CH), 139.8 (d, ^2J(C,P) = 21 Hz, C4), 140.5, 155.8 (2s, C_{ipso} of the phenyls), 141.5 (d, ^1J(C,P) = 44.5 Hz, C2), 151.2 ppm (d, ^1J(C,P) = 25.7 Hz, C5); ^{31}P NMR ($CDCl_3$, 121.5 MHz): $\delta = -8.3$ ppm; MS (IE): m/z: 453 [M^++1].

1-Phospha-2-triethoxysilyl-4,5-dimethyl-3,6-diphenylnorbornene (2′): Triethoxysilane (1.64 g, 10 mmol) and $PtCl_2$ (26 mg, 0.1 mmol) were added to a solution of phenylacetylene (1.02 g, 10 mmol) in ethanol (15 mL). The solution was stirred at 50 °C for 12 h. The solvent was removed in vacuo. ^{1}H NMR showed a total conversion of the alkyne to *cis*-triethoxystyrylsilane and triethoxy(1-phenylvinyl)silane in a 2:1 ratio. 1-Phenyl-3,4-dimethylphosphol (1.29 g, 6.6 mmol) was added to the reaction products without solvent and the mixture was heated in a sealed tube at 140 °C for 4 h. ^{31}P NMR showed that only one product was formed. The unreacted triethoxy(1-phenylvinyl)silane was removed by Kugelrohr distillation. The product was isolated as a colorless oil. Yield: 1.1 g (60%); ^{1}H NMR ($CDCl_3$, 300 MHz): $\delta = 1.0$ (t, ^3J(H,H) = 8 Hz, 9H; CH_3), 1.2 (s, 3H; CH_3), 1.3 (s, 3H; vinylic CH_3), 1.5 (m, 2H; CH_2), 3.0 (d, J(H,P) = 7 Hz, 1H, Si–CH), 3.6 (m, 6H; OCH_2), 7.0, 7.2–7.5 ppm (d, J(H,H) = 7 Hz, 2H; m, 8H; phenyls); ^{13}C NMR ($CDCl_3$, 75.5 MHz): δ = 16.5 (s, vinylic CH_3), 18.3 (s, CH_3 of the ethoxy moieties), 21.0 (s, CH_3), 28.2 (d, ^2J(C,P) = 29 Hz, C1), 50.4 (s, CH_2), 53.3 (s, C2), 59.0 (s, OCH_2), 65.5 (s, C3), 126.5–129.5 (4s, aromatic CH), 139.2 (d, ^2J(C,P) = 20.4 Hz, C4), 142.6, 151.3 (2s, C_{ipso} of the phenyls), 143.4 ppm (d, ^1J(C,P) = 21.9 Hz, C2); ^{31}P NMR ($CDCl_3$, 121.5 MHz): $\delta = -14.9$ ppm; MS (IE): m/z: 455 [M^++1].

1-Phospha-2-ethoxydimethylsilyl-4,5-dimethyl-3,6-diphenylnorbornadiene (4): A solution of ethoxydimethyl(phenylethynyl)silane (1.02 g, 5 mmol) and 1-phenyl-3,4-dimethylphosphol(0.96 g, 5 mmol) in xylene (5 mL) was heated in a sealed tube at 140 °C for 4 h. The reaction mixture is filtered on celite and the xylene was removed in vacuo. The product was isolated as a colorless oil. Yield: 1.6 g (90%); ^{1}H NMR ($CDCl_3$, 300 MHz): δ = 0.0, 0.04 (s, 6H, Si–CH_3), 1.1 (t, ^3J(H,H) = 7 Hz, 9H; CH_3), 1.4 (s, 3H; CH_3), 2.1 (m, 2H; CH_2), 2.2 (s, 3H; vinylic CH_3), 3.5 (q, ^3J(H,H) = 7 Hz, 2H; OCH_2), 7.0, 7.2–7.5 ppm (d, J(H,H) = 5 Hz, 2H; m, 8H; phenyls); ^{13}C NMR ($CDCl_3$, 75.5 MHz): δ = 0.0 (s, Si–CH_3), 16.5 (s, vinylic CH_3), 19.0 (s, CH_3 of the ethoxy moieties), 20.9 (s, CH_3), 59.0 (s, OCH_2), 67.5 (s, CH_2), 74.2 (s, C3), 126.7–128.8 (4s, aromatic CH), 132.5 (s, C2), 139.9 (d, ^2J(C,P) = 12.8 Hz, C4), 141.3, 156.8 (2s, C_{ipso} of the phenyls), 151.0 (d,

^1J(C,P) = 25.7 Hz, C1), 156.7 ppm (d, ^1J(C,P) = 14.3 Hz, C5); ^{31}P NMR ($CDCl_3$, 121.5 MHz): $\delta = -12.1$ ppm; MS (IE): m/z: 393 [M^++1].

1-Oxo-1-phospha-4,5-dimethyl-3,6-diphenylnorbornadienyl phosphonic acid (5′): Aqueous HNO_3 (1 mL, 15 M, 15 mmol) was added to **5** (370 mg, 1 mmol) in methanol. After 15 min the reaction mixture was neutralized with aqueous $NaHCO_3$ and extracted with CH_2Cl_2. The organic phase was dried over $MgSO_4$ and the solvent was removed in vacuo. The product was isolated as white crystals. Yield: 200 mg (55%); ^{1}H NMR ($CDCl_3$, 300 MHz): $\delta = 1.2$ (s, 3H; CH_3), 2.0 (s, 3H; vinylic CH_3), 3.4 (m, 2H; CH_2), 7.0, 7.1–7.5 ppm (s, 2H; m, 8H; phenyls); ^{13}C NMR ($CDCl_3$, 75.5 MHz): $\delta = 14.4$ (s, vinylic CH_3), 17.5 (s, CH_3), 67.5 (d, ^1J(C,P) = 37.8 Hz, CH_2), 67.2 (d, ^3J(C,P) = 71.0, C3), 126.2–129.2 (aromatic CH), 130.0 (m, C2), 133.7 (m, C4), 151.0 (d, ^1J(C,P) = 25.7 Hz, C1), 159.3 ppm (m, C5); ^{31}P NMR ($CDCl_3$, 121.5 MHz): $\delta = 10.3$ (d, ^2J(P,P) = 31.6 Hz; $-PO_3H_2$), 51.7 ppm (d, ^2J(P,P) = 31.6 Hz; −P=O); MS (IE): m/z: 387 [M^++1].

Silica supports: Structural characteristics of **SBA-1**, **SBA-15**, and **MSU** are summarized in Table 6.

Table 6. Structural characteristics of **SBA-1**, **SBA-15**, and **MSU**.

Powder	Specific surface area [m^2g^{-1}]	Average pore diameter [Å]	XRD (d spacing) [nm]
SBA-1	730	28	3.4
SBA-15	540	80	9.2
MSU	310	100	–

SBA-1:[12] In a typical run, cetyltriethylammonium bromide (1.2 g) was dissolved at room temperature in aqueous HCl solution (61 mL, 3.6 M). TEOS (5.2 g) was then added with vigorous stirring. After 1 h a white powder began to be precipitated; after 3 h precipitation was complete. The powder was filtered off and washed three times with distilled water. After 48 h of consolidation at 110 °C, the surfactant was removed by a 24 h ethanolic Soxhlet extraction. A 4 h calcination step at 450 °C ensured complete removal of surfactant.

SBA-15 and MSU: **SBA-15** was synthesized according to reference [13], and synthesis of **MSU** was as described in reference [14].

Mixed zirconia/silica supports

Sol A: Cetyltrimethylammonium bromide (0.625 g) was dissolved in ethanol (18.2 g). Zirconium tetrachloride (2.33 g) was then added with vigorous stirring.

Sol B: Cetyltrimethylammonium bromide (0.625 g) was dissolved in ethanol (18.2 g). Silicon tetrachloride (1.68 g) was then added slowly with vigorous stirring, in order to avoid evolution of HCl.

Mixture: Sols A and B were mixed in a volume ratio corresponding to the desired Zr/Si molar ratio and then atomized.

Grafting procedure

Silica material: In a typical run the appropriate silica powder (100 mg) was suspended in toluene (20 mL) under argon. The phosphine to be grafted (50 mg) was added. The solution was heated at 90 °C for 12 h with vigorous stirring. The powder was filtered off and submitted to a 12 h ethanolic Soxhlet extraction, under nitrogen. The resulting powder was dried under vacuum for 12 h.

Mixed zirconia/silica material: In a typical run the appropriate silica powder (100 mg) was suspended in methanol (5 mL) under argon. The phosphinic acid (20 mg) to be grafted and triphenylphosphine (5 mg) were added. The solution was heated at 90 °C for 12 h with vigorous stirring. The powder was filtered off and the grafting rate was checked by integration of the ^{31}P NMR spectra of the solution (with PPh_3 as an internal standard) and submitted to a 12 h ethanolic Soxhlet extraction, under nitrogen. The resulting powder was dried under vacuum for 12 h.

Catalytic tests

Complexation: The rhodium precursor (either $[Rh(cod)_2][PF_6]$ or $[Rh(acac)(CO)_2]$, 1 equiv) was added to a suspension of the given material (20 mg) in dichloromethane (5 mL) under argon. After 30 min of stirring, the powder was centrifuged and washed with dichloromethane (5 mL).

Hydrogenation: Hexene (0.84 g, 1 mmol) was dissolved in MeOH (20 mL). The weight of the catalyst added corresponded to a theoretical substrate/Rh molar ratio of 1:1000. The mixture was introduced to a stainless steel autoclave fitted with a glass vessel, degassed, and pressurized at 7 bar. The mixture was stirred vigorously at room temperature. The yield was determined by GC.

Hydroformylation: 2,3-Dimethylbut-2-ene (0.84 g, 1 mmol) was dissolved in toluene (20 mL). The weight of catalyst added corresponded to a theoretical substrate/Rh molar ratio of 1:1000. The mixture was introduced to a stainless steel autoclave, degassed, and pressurized at 30 bar of H_2/CO (1:1) mixture. The mixture was stirred vigorously at 110 °C for 48 h. The yield was determined by GC and confirmed by ^{1}H NMR spectroscopy.

Computational details: All computations were performed using the Gaussian 03 suite of programs and gradient-corrected density functional theory[29] by using the B3PW91 functional.[30] Optimizations of **I** and **II** were carried out using the 6-311+G(d) basis set for the atoms constituting the P–C–Si–O chelate motif and the 6-31G* basis set for all other atoms. The basis set employed for the rhodium atom incorporates the Hay and Wadt small-core relativistic effective core potential and double-zeta valence basis set (441/2111/31/1).[31] The exponent for the metal f function applied is 1.350.[32] The same basis sets were employed for the calculations of structures **III** and **IV**, the 6-311+G(d) basis set being employed for the C and H atoms of the two coordinated ethylene ligands. The charge distribution in optimized structures was calculated with the NBO partitioning scheme.[33] Minima were characterized by having no imaginary frequency.

Acknowledgements

We are grateful to the Saint-Gobain Recherche Company for funding. The CNRS, the Pierre et Marie Curie University, and the École Polytechnique are thanked for supporting this work. The IDRIS Center (Orsay, Paris XI) is gratefully acknowledged for the allowance of computer time. C.S. wants to thank the dog and the goldfish.

[1] B. Cornils, W. A. Herrmann, *J. Catal.* **2003**, *216*, 23–31.
[2] J. A. Gladysz, *Chem. Rev.* **2002**, *102*, 3215–3216.
[3] J. S. Beck, J. C. Vartuli, W. J. Roth, M. E. Leonowicz, C. T. Kresge, K. D. Shmitt, C. T. W. Chu, D. H. Olson, E. W. Sheppard, S. B. McCullen, J. B. Higgins, J. L. Schlenker, *J. Am. Chem. Soc.* **1992**, *114*, 10834–10843.
[4] A. Corma, *Chem. Rev.* **1997**, *97*, 2373–2419.
[5] A. Choplin, F. Quignard, *Coord. Chem. Rev.* **1998**, *178*, 1679–1702.
[6] C. Copéret, M. Chabanas, R. Petroff Saint-Arroman, J.-M. Basset, *Angew. Chem.* **2003**, *115*, 164–191; *Angew. Chem. Int. Ed.* **2003**, *42*, 156–181.
[7] F. Goettmann, D. Grosso, F. Mercier, F. Mathey, C. Sanchez, *Chem. Commun.* **2004**, 1240–1241.
[8] G. J. D. Soler-Illia, C. Sanchez, B. Lebeau, J. Patarin, *Chem. Rev.* **2002**, *102*, 4093–4138.
[9] F. Mathey, F. Mercier, C. Charrier, J. Fischer, A. Mitschler, *J. Am. Chem. Soc.* **1981**, *103*, 4595–4597.
[10] N. Mézailles, N. Maigrot, S. Hamon, L. Ricard, F. Mathey, P. Le Floch, *J. Org. Chem.* **2001**, *66*, 1054–1056.
[11] S. Lelièvre, F. Mercier, F. Mathey, *J. Org. Chem.* **1996**, *61*, 3531–3533.
[12] V. Goletto, V. Dary, F. Babonneau, *Mater. Res. Soc. Symp. Proc.* **1999**, 576.

[13] D. Y. Zhao, J. L. Feng, Q. S. Huo, N. Melosh, G. H. Fredrickson, B. F. Chmelka, G. D. Stucky, *Science* **1998**, *279*, 548–552.
[14] C. Boissière, A. Larbot, E. Prouzet, *Chem. Mater.* **2000**, *12*, 1937–1940.
[15] Z. G. Wu, Y. X. Zhao, Y. H. Liu, *Microporous Mesoporous Mater.* **2004**, *68*, 127–132.
[16] G. Soler-Illia, E. L. Crepaldi, D. Grosso, C. Sanchez, *J. Mater. Chem.* **2004**, *14*, 1879–1886.
[17] D. Carrière, M. Moreau, P. Barboux, J. P. Boilot, O. Spalla, *Langmuir* **2004**, *20*, 3449–3455.
[18] G. Guerrero, P. H. Mutin, A. Vioux, *Chem. Mater.* **2001**, *13*, 4367–4373.
[19] "^{31}P Nuclear Magnetic Resonance": M. M. Crutchfield, C. H. Dungan, J. H. Letcher, V. Mark, J. R. van Wazer, *Topics in Phosphorus Chemistry*, Wiley-Interscience, New York, **1967**.
[20] S. L. Buchwald, R. B. Nielsen, *Chem. Rev.* **1988**, *88*, 1047–1058.
[21] D. W. Sindorf, G. E. Maciel, *J. Am. Chem. Soc.* **1983**, *105*, 1487–1493.
[22] C. Sanchez, F. Ribot, *New J. Chem.* **1994**, *18*, 1007–1047.
[23] a) B. Breit, R. Winde, T. Mackewitz, R. Paciello, K. Harms, *Chem. Eur. J.* **2001**, *7*, 3106–3121; b) A. Moores, N. Mézailles, L. Ricard, P. Le Floch, *Organometallics* **2005**, *24*, 508–513.
[24] G. C. Ossenkamp, J. H. Kemmit, J. H. Johnston, *Langmuir* **2002**, *18*, 5749–5754.
[25] C. J. Brinker, G. W. Scherer, *Sol–Gel Science: The Physics and Chemistry of Sol–Gel Processing*, Academic Press, San Diego, **1990**.
[26] a) D. E. Fogg, E. N. dos Santos, *Coord. Chem. Rev.* **2004**, *248*, 2365–2379; b) J.-C. Wasilke, S. J. Obrey, R. T. Baker, G. C. Bazan, *Chem. Rev.* **2005**, *105*, 1001–1020.
[27] a) F. Gelman, J. Blum, D. Avnir, *New J. Chem.* **2003**, *27*, 205–207; b) F. Gelman, J. Blum, D. Avnir, *J. Am. Chem. Soc.* **2002**, *124*, 14460–14463; c) F. Gelman, J. Blum, H. Schumann, D. Avnir, *J. Sol–Gel Sci. Technol.* **2003**, *26*, 43–46; d) F. Gelman, J. Blum, D. Avnir, *Angew. Chem.* **2001**, *113*, 3759–3761; *Angew. Chem. Int. Ed.* **2001**, *40*, 3647–3649; e) F. Gelman, J. Blum, D. Avnir, *J. Am. Chem. Soc.* **2000**, *122*, 11999–12000.
[28] a) M. D. Martinez-Ortiz, D. Tichit, P. Gonzalez, B. Coq, *J. Mol. Catal. A* **2003**, *201*, 199–210; b) D. Tichit, B. Coq, S. Cerneaux, R. Durand, *Catal. Today* **2002**, *75*, 197–202.
[29] M. J. Frisch, G. W. Trucks, H. B. Schlegel, G. E. Scuseria, M. A. Robb, J. R. Cheeseman, V. G. Zakrzewski, J. J. A. Montgomery, R. E. Stratmann, J. C. Burant, S. Dapprich, J. M. Millam, A. D. Daniels, K. N. Kudin, M. C. Strain, O. Farkas, J. Tomasi, V. Barone, M. Cossi, R. Cammi, B. Mennucci, C. Pomelli, C. Adamo, S. Clifford, J. Ochterski, G. A. Petersson, P. Y. Ayala, Q. Cui, K. Morokuma, D. K. Malick, A. D. Rabuck, K. Raghavachari, J. B. Foresman, J. Cioslowski, J. V. Ortiz, A. G. Baboul, B. B. Stefanov, G. Liu, A. Liashenko, P. Piskorz, I. Komaromi, R. Gomperts, R. L. Martin, D. J. Fox, T. Keith, M. A. Al-Laham, C. Y. Peng, A. Nanayakkara, M. Challacombe, P. M. W. Gill, B. Johnson, W. Chen, M. W. Wong, J. L. Andres, C. Gonzalez, M. Head-Gordon, E. S. Replogle, J. A. Pople, Gaussian 98, Revision A-11, Gaussian, Inc., Pittsburgh (PA), **1998**.
[30] A. D. Becke, *J. Chem. Phys.* **1993**, *98*, 5648.
[31] P. J. Hay, W. R. Wadt, *J. Chem. Phys.* **1985**, *82*, 299–310.
[32] A. Ehlers, M. Bohme, S. Dapprich, A. Gobbi, A. Hollwarth, V. Jonas, K. Kohler, R. Stegmenn, A. Veldkamp, G. Frenking, *Chem. Phys. Lett.* **1993**, *208*, 111.
[33] A. E. Reed, L. A. Curtiss, F. Weinhold, *Chem. Rev.* **1988**, *88*, 899–926.
[34] P. van Leeuwen, A. J. Sandee, J. N. H. Reek, P. C. J. Kamer, *J. Mol. Catal. A* **2002**, *182*, 107–123.

Received: May 16, 2005
Published online: October 14, 2005

